Int J Adv Manuf Technol (2018) 94:2301–2313
DOI 10.1007/s00170-017-0932-7

ORIGINAL ARTICLE

# Quasi-static analysis of mechanical properties of Ti6Al4V lattice structures manufactured using selective laser melting

**Qixiang Feng[1] · Qian Tang[1] · Ying Liu[2] · Rossi Setchi[2] · Shwe Soe[2] · Shuai Ma[1] · Long Bai[1]**

Received: 17 January 2017 / Accepted: 8 August 2017 / Published online: 7 September 2017
© Springer-Verlag London Ltd. 2017

**Abstract** Selective laser melting (SLM) is a transformative manufacturing process due to its ability to manufacture complex metal parts directly from various bulk powders. With the capability of reducing powder consumption and decreasing fabrication times, lattice structures, which are used as infilling materials within hollow parts, offer an effective solution for decreasing the high costs that currently impede the wider application of SLM in various industries. The assessment of mechanical properties of SLM-built lattice structures, however, remain challenging due to their complicated geometries, while pursuing experimental studies proves to be time-consuming due to the requirement of numerous part fabrication and physical testing. To address these research challenges, this study proposes an analytical modelling approach conducting quasi-static analysis on Ti6Al4V (Ti64) lattice structures. In order to investigate the structures' mechanical properties, dynamic balance equation of the structures under compression loads were first established, and the stress distribution of the structures was calculated explicitly using central difference method. The modelling approach was validated by conducting uniaxial compression tests on samples fabricated using SLM. The experiments showed that the equivalent elastic modulus ($E^*$) and the ultimate stress ($UTS$) values of the Ti64 structures predicted by the analytical method were in good agreement with the experimental results. The paper also discusses the design principles of SLM-built lattice structures (mainly the selection of proper topologies and relative densities) and examines the necessity and flexibility of the proposed analytical approach compared with conventional theoretical methods and their experimental studies in the context of SLM process.

**Keywords** Selective laser melting · Ti6Al4V · Lattice structure · Analytical modelling

✉ Qian Tang
tqcqu@cqu.edu.cn

[1] College of Mechanical Engineering, Chongqing University, NO. 174 Shazheng Street, Shapingba District, Chongqing 40044, China

[2] School of Engineering, Cardiff University, Queen's Building, Newport Road, Cardiff CF24 3AA, UK

## 1 Introduction

Complex metallic parts fabricated using selective laser melting (SLM), has been widely used for various applications in the aerospace [1] and medical industries [2]. Commercial SLM systems generally use fibre lasers of 200 W to 1 KW to selectively melt metal powders layer by layer in a build chamber filled with nitrogen or argon to prevent an oxidation reaction from occurring with the metal powders. Laser power, scanning speed, laser spot diameter, hatching space and layer thickness are some of the key processing parameters. To guarantee the final part's density, the thickness of each melting layer is usually set to be in the range of 20–100 μm (as determined by the laser power) once the bulk powder type is selected. Various bulk materials have been shown to be suitable for this manufacturing process, including titanium [3, 4], cobalt chrome alloy [5], aluminium [6, 7], stainless steel [8, 9], invar [10] and even pure gold [11]. Of the wide range of powders used in SLM, Ti6Al4V (Ti64) powders have been successfully applied in fabricating parts with superior properties such as high strength-to-weight ratio, erosion-resistance and biocompatibility.

The high cost of SLM processes remains an impediment to wider industrial implementation of SLM-built Ti64 parts, due to a high consumption of the powders and the depreciation

expense of the system. Like other laser-based powder-bed fusion/melting systems, a SLM process is time-consuming, since its highest fabrication rate is ~ 100 $cm^3$/h (e.g. EOS M 400-4, an ultra-fast SLM system with four lasers). Today, the fabrication of dense Ti64 parts at the centimetre scale usually requires at least 10 h of processing time, thus leading to extravagant depreciation expenses. Because both industry and academia have long sought to manufacture large Ti64 components at the metre scale, it is necessary to explore an effective solution for lowering powder consumption and decreasing manufacturing times (and thus costs).

This challenge may be addressed during the Ti64 parts' design stage. One advantage of SLM, for instance, is that components could be designed to be hollow-like and lightweight using an infilling method, where the shape is unchanged and the inner section is in-filled with porous structures [12], if the components are to be used in low-stress applications. Lattice structures, which consist of well-organised microscale unit cells, are quite suitable to be the filled medium for the data-driven SLM process.

Numerous experimental studies have been conducted in order to better understand the mechanical properties of the SLM-built Ti64 lattice structures. However, this trial-and-error approach is expensive, since it requires numerous SLM-built samples to be printed and tested. In order to decrease the costs of experimental studies and to better guide the design of SLM-built Ti64 lattice structures, this paper hence proposes an analytical modelling approach for conducting quasi-static analysis on compression behaviours of the structures. Since the deformation and stress distribution of the structures were obtained by solving explicitly the dynamic balance equation of the compressed structures, which includes complex geometrical features, large deformation and complicated contact, using this approach can better ensure that the solution process is stable and easy to converge.

The remainder of this paper is structured as follows. Section 2 discusses related works on SLM-built Ti64 lattice structures, Sect. 3 introduces a quasi-static analytical modelling approach that was applied on two typical lattice structures, and Sect. 4 presents quasi-static tensile and compression experiments in order to verify the feasibility of the proposed method. Sections 5 presents an analysis of the results and a discussion of the study. The final section includes conclusions and discusses opportunities for further research.

## 2 Related works

This section reviews relevant research on SLM-built Ti64 lattice structures, with a particular focus on the SLM process and the methods used to predict mechanical properties of metallic lattice structures.

### 2.1 The SLM process used for Ti64 lattice structures

Metallic lattice structures have been manufactured using conventional manufacturing processes such as casting [13–15]; however, these conventional processes have certain drawbacks. First, they require various complicated and time-consuming procedures, and the geometrical features and unit-cell sizes are both limited [16]. Second, because conventional processes require metallic materials with good manufacturability, it is difficult to fabricate Ti64 lattice structures under these conditions. In contrast, metal additive manufacturing (AM) processes, such as powder-feed AM (e.g. the robotized laser-based metal AM [17]), electron beam melting (EBM) [18] and selective laser melting (SLM), allow the fabrication of Ti64 lattice structures in relatively short times (thus saving on costs) and at the micrometre scale. SLM and EBM are powder-bed system, loose powders supporting melting parts during a fabrication process, and hence, SLM and EBM can manufacture complex 3D porous structures, while it is difficult to fabricate these structures using powder-feed AM processes due to a lack of effective supporting structures. Meanwhile, when fabricating Ti64 parts, SLM-produced samples exhibit better surface accuracy, higher tensile strength and higher fatigue limit than EBM-produced samples [19]. Therefore, these SLM-built Ti64 microstructures are widely used to design bone substitutes in biomedical studies, for example, due to these structures' modulus-matching abilities with peripheral tissues [20], good bioactivity after proper surface-treatment procedures [21] and adequate fatigue behaviour in vivo environments [22, 23].

SLM-built Ti64 parts also exhibit several unique mechanical properties compared with their counterparts fabricated by traditional means. The rapid-heating-and-cooling manufacturing process induces martensitic $\alpha'$ microstructures in as-produced Ti64 parts [24], which leads to a high elastic modulus in excess of 900 MPa within SLM-built dense Ti64 parts [25]. As a consequence, the as-produced Ti64 lattice structures provide high strength, thus providing superior lightweight properties compared to their SLM-built stainless-steel counterparts.

Ti64 lattice structures exhibit brittle behaviour when fracture analysis is conducted [25], which suggests that the Ti64 structures are suitable in supporting applications. In addition, the mechanical properties of Ti64 structures are dependent on the build orientation [26]. In order to fabricate Ti64 structures that are free from obvious pores and stratification, the process parameters must be optimised, similarly to the measurements conducted with dense Ti64 parts [27]. In addition, because bulk powders easily adhere to the adjacent melting pools during the manufacturing process, rough surfaces and geometric discrepancies between computer-aided design (CAD) models and as-produced parts are engendered [28], such as uneven geometrical and mechanical properties along the struts of Ti64

structures [29]. This geometric discrepancy between CAD models and as-produced structures can be minimised by controlling the process parameters to decrease the adhered powders on struts [30, 31], or by modifying the design sizes of the CAD models according to the images obtained by use of a micro-CT-based design method [32].

### 2.2 Prediction of the mechanical properties of SLM-built lattice structures

Mechanical properties of Ti64 lattice structures built using SLM can be accurately assessed using experimental study [33]. However, the necessity for repeated tests when conducting experimental studies leads to high manufacturing costs. Therefore, there is a need to conduct a theoretical analysis or analytical simulations prior to conducting expensive sample tests. Common theoretical methods treat the strut as an Euler-Bournelli or Timoshenko beam and estimate the structure's mechanical properties based on the deformation of unit cells when the structure undergoes a stress condition [34–36]. However, this approximation method cannot provide detailed stress-distribution characteristic at joints and constraints. This method also requires the use of structures with good symmetrical properties at the strut level, such as body-centred cubic (BCC)-type and diamond-type structures. Additionally, this method states that the structure needs to be homogeneous in nature consisting of straight struts only, and as a consequence, it is impractical to analyse more complicated structures consisting of curved struts (such as is the case with gyroid-type structures) [37] or the variable-density lattice structures [38].

These various drawbacks indicate that this theoretical method lacks universality, since lattice structures with various geometrical features have been fabricated using SLM in past studies. With an increase in computational efficiency, researchers have been able to employ analytical modelling methods to evaluate the mechanical performance of complex lattice structures [16, 39]. The complexity involved in a lattice structure generation, however, depends on the cell type, size, the number of repeat units required to fill the empty volume and the conforming desirability of the adjacent boundaries. The successful analytical simulation requires many considerations such as the adaptation of correct analysis type, the selection of right material model and finally the trade-off between the accuracy demanded and economical solution achievable.

Therefore, to improve the computing speed and reliability of the simulation, this paper proposed a quasi-static analytical method to calculate the mechanical properties of SLM-built Ti64 lattice structures. The dynamical model of the structures, which are sustaining compression loads, was established first. Then, the displacement matrices of the structures were solved using the central difference method. The stress and the strain matrices were calculated and the stress-strain curves of the structures were obtained. These curves were compared with their counterparts obtained via quasi-static compression tests. Both the validity and any shortcomings of the proposed simulation method were evaluated.

## 3 Proposed analytical modelling approach for Ti64 lattice structures.

This section presented an analytical modelling approach that was developed to model the mechanical properties of two types of SLM-built Ti64 lattice structures and to estimate the stress distribution of these structures. The section first introduced the selection of topologies of the structure before presenting in detail the proposed analytical modelling method.

### 3.1 Topology characterisation

Although BCC lattice structures are quite common in the design of SLM-produced lattice structures, few previous studies have explained the rationale of adopting this typical topology. A BCC unit cell may be obtained by connecting a set of feature points on a cube. As Fig. 1a–c shows, the feature points in a cube are categorised as one body-centred point, eight peaks, eight face-centred points and 12 midpoints of 12 edges, as shown in Fig. 1. A strut is then obtained by connecting two feature points, which results in numerous unit cells.

Due to the symmetry of the shape, it is reasonable to consider only one-eighth of the previous cube, which yields a new cube with eight peaks in this case, as shown in Fig. 1d. Thus, as Fig. 1e shows, the most complicated unit cells are obtained in cases where all eight feature points are connected to one another as possible struts. All the struts perpendicular to three axes are removed by considering the poor manufacturability of the cantilever beams, then this complicated unit cell is simplified to the more commonly seen BCC unit cell. The BCC lattice structures are obtained using a repeat-and-stack method, as shown in Fig. 1f, g. The BCC structures are isotropic following this process. The equivalent elastic modulus ($E^*$) can then be calculated proximately as shown in Eq. (1), which was obtained based on the beam-theory method proposed in [28]:

$$E^* = \frac{9\sqrt{3}E\pi}{4\left(l/d\right)^2\left[3+8\left(l/d\right)^2\right]} \tag{1}$$

where $E$ is the elastic modulus of the bulk material, and $l$ and $d$ represent the length and diameter of the strut, respectively. Equation (1) is rewritten as follows when $l >> d$:

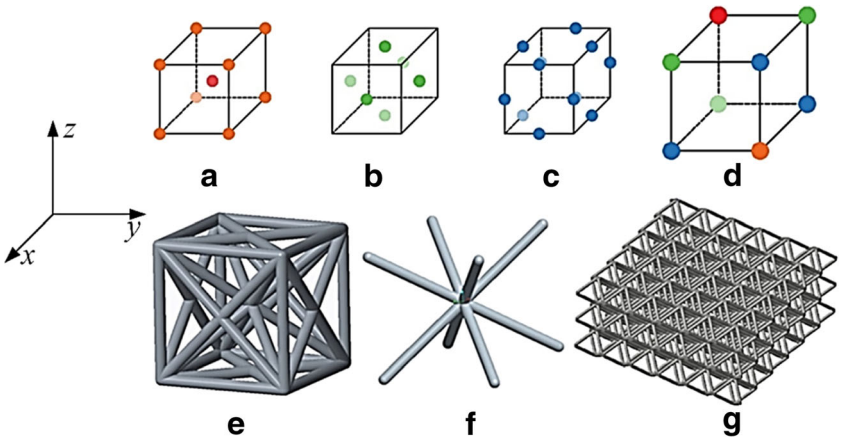


**Fig. 1** The formation of the BCC-type lattice structures based on the feature points of a cube

$$E^* = CE\left(d/l\right)^4 \tag{2}$$

where $C$ is a constant.

In certain applications that require a large unidirectional bearing capability (which BCC structures cannot provide), some additional struts are superposed on a BCC unit cell to form a so-called unidirectional reinforced lattice structure. As Fig. 2a shows, an fcc-BCC unit cell is obtained when an FCC unit cell (yellow colour) is added to an enclosed BCC unit cell (in grey). As Fig. 2b shows, this results in more complicated structures, which would be difficult to calculate using the similar equation that are adopted with BCC structures. The quasi-static analytical method proposed in the following subsection, however, can solve this problem.

### 3.2 Quasi-static analytical method for SLM-built Ti64 lattice structures

CAD models of the aforementioned two types of Ti64 lattice structures were built, and each type of structure had four relative densities. For each BCC-type structure, the aspect ratio (AR) of the struts (the ratio of the strut length to its diameter) was set to be 10, 8, 6 and 4. For each fcc-BCC-type structure, the AR was defined as the ratio of the length to the diameter of the longest struts. The sizes of the unit cells were determined by considering the manufacturing accuracy of the used SLM system. In this paper, the edge size of the unit cell was 5 mm, and the minimum diameter of the struts in the structure with AR = 10 was ~ 0.43 mm. As Figs. 1g and 2b show, there were six unit cells along the directions of length and width, while there were three unit cells in the height direction, which was parallel to the build orientation in the SLM system.

Due to the symmetry of the CAD models, one-quarter symmetric analytical models were established, as shown in Fig. 3. To obtain internal stress distribution of a lattice structure when sustaining compressive load, its dynamic balance equation was established as

$$[M]\{\ddot{u}\} + [C]\{\dot{u}\} + [K]\{u\} = \{P\} \tag{3}$$

where $[M]$, $[C]$ and $[K]$ are mass matrix, damping matrix and stiffness matrix, respectively. $\{\ddot{u}\}$, $\{\dot{u}\}$, and $\{u\}$ are acceleration matrix, velocity matrix and displacement matrix, respectively. $\{P\}$ is the force matrix sustained by the structure.

$\{u\}$, $\{\dot{u}\}$ and $\{\ddot{u}\}$ were calculated analytically at any given time $t$ through the above equation using central difference method, where $\{\ddot{u}\}$ and $\{\dot{u}\}$ at time $t$ are

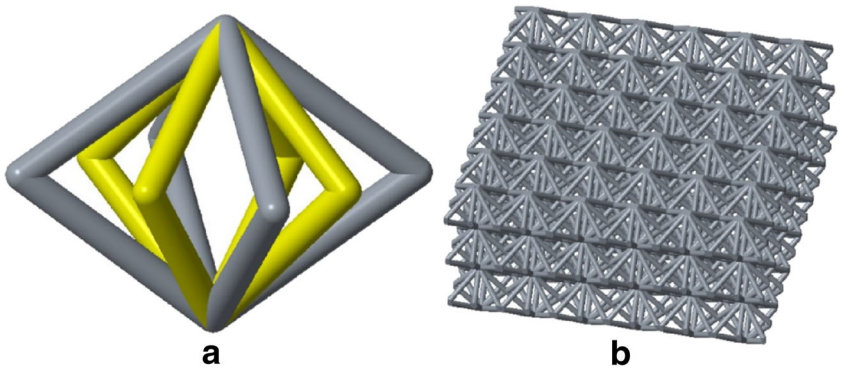


**Fig. 2** The fcc-BCC unit cell and the fcc-BCC lattice structures

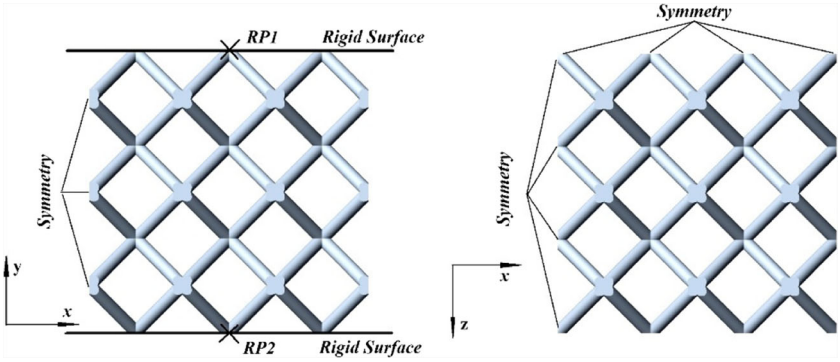


**Fig. 3** Quasi-static analytical model of a BCC lattice structure and its boundary conditions

$$\{\ddot{u}\}_t = \frac{1}{\Delta t^2}\left(\{u\}_{t-\Delta t} - 2\{u\}_t + \{u\}_{t+\Delta t}\right) \tag{4}$$

$$\{\dot{u}\}_t = \frac{1}{2\Delta t}\left(\{u\}_{t+\Delta t} - \{u\}_{t-\Delta t}\right) \tag{5}$$

When $t = 0$,

$$\{\dot{u}\}_{0-\Delta t} = \{u\}_0 - \Delta t\{\dot{u}\}_0 + \frac{\Delta t^2}{2}\{\ddot{u}\}_0 \tag{6}$$

The above-mentioned analytical method requires a definite total analysing time period, which was determined by conducting frequency analysis on the corresponding structure. Let $[C]$ and $\{P\}$ be zero, then

$$[M]\{\ddot{u}\} + [K]\{u\} = 0 \tag{7}$$

The general solution of Eq. (7) is

$$\{u\} = \{\phi\}sinwt \tag{8}$$

where $\{\phi\}$ is a eigenvector, and $w$ is natural frequency corresponding to $\{\phi\}$.

From Eqs. (7) and (8), let $\lambda = \omega^2$, then

$$([K] - \lambda[M])\{\phi\} = 0 \tag{9}$$

By solving Eq. (9), the second-order natural frequency of the structure was obtained, and the second-order frequency was then used to calculate the minimum time period (MTP). The actual time period of each model was set to be two or three times that of the MTP, thus ensuring the success of the quasi-static analysis and avoiding a time-consuming analytical process due to arbitrary and unreasonable time periods.

The analytical models for prediction of lattice structures were established using ABAQUS. As shown in Fig. 3, two symmetric boundary conditions were established. The compression load was applied using the displacement technique. Two rigid surfaces with two reference points (RPs) were built to simulate the compression head and the bottom surface of the testing machine. During the simulation process, RP1 moved downward by 5 mm, while RP2 remained in place. The displacement load was applied gradually in order to guarantee the accuracy of the quasi-static analysis, which complied with a smooth-step curve related to the above-mentioned time period.

## 4 Experimental study

This section presents the quasi-static tensile tests that were conducted on SLM-produced Ti64 tensile specimens

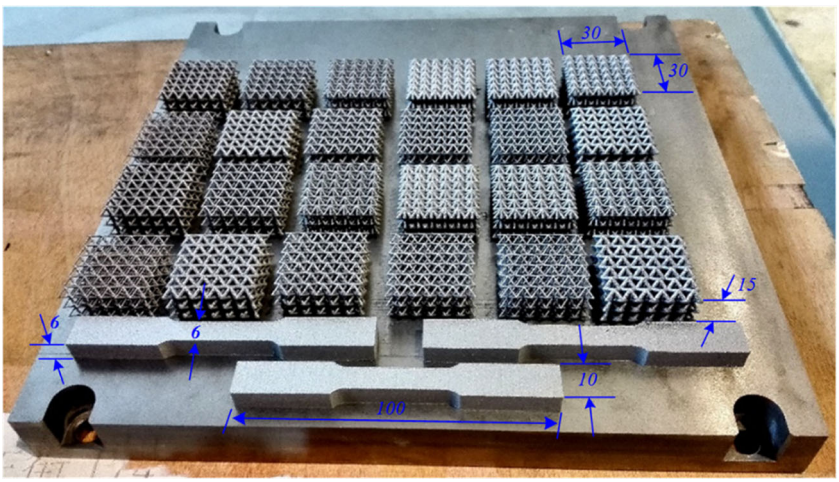


**Fig. 4** Ti64 parts on a substrate fabricated via SLM

**Table 1** Manufacturing parameters adopted in the SLM process

| Laser power | Laser diameter | Scanning speed | Hatching space | Layer thickness |
|---|---|---|---|---|
| 170 W | 100 μm | 1250 mm/s | 100 μm | 30 μm |

in order to obtain the material properties required by Eq. (3). The CAD models which were established in Sect. 3 were exported as STL files and imported to an SLM system (EOS M280). As Fig. 4 shows, the tensile specimens and lattice structure samples were fabricated on a substrate board.

The manufacturing parameters that were adopted are shown in Table 1. The specimens and samples were subjected to a stress-relief heat treatment, where the fabricated parts were heated to 750 °C; the temperature was then maintained for 2 h and cooled in a vacuum. Quasi-static compression tests were then conducted on BCC-type and fcc-BCC-type Ti64 lattice structures, respectively.

### 4.1 Quasi-static tensile test

The tensile specimens were modelled in accordance with ASTM E8/E8M-15a: 'Standard Test Methods for Tension Testing of Metallic Materials'; the specimens were categorised as sub-size specimens. After fabrication via SLM, the three identical specimens were machined to meet ASTM size standards. To avoid any slippage between the specimen and the clamps during the tensile process, sandblasting was conducted on the surfaces of the two ends of each specimen, and an extensometer was used to accurately record the displacement of the specimen, as shown in Fig. 5a, b. The tensile rate was 2 mm/s for all three of the tests that were conducted on the three tensile specimens.

### 4.2 Quasi-static compression test

Figure 6 shows the SLM-built Ti64 lattice structures and an image of the quasi-static compression test that was conducted on a structure sample. The compression rate was 1 mm/min, and the compression load was applied along the build orientation of structures. The reaction force that was sustained by the compression crosshead and its displacement were recorded during each test; the nominal stress-strain diagrams were then plotted based on this data.

## 5 Results

This section first illustrates the material properties of the SLM-produced Ti64 parts. The subsections that follow then compare the mechanical properties of the lattice structures—including the equivalent elastic modulus ($E^*$) and the ultimate strength ($UTS$)—that were obtained via the quasi-static analytical method and experimental study. After presenting the stress distribution of Ti64 lattice structures obtained via the quasi-static analysis, the section concludes with a general discussion of some of the design principles of Ti64 lattice structures based on the results presented in this paper.

### 5.1 Characterisation of Ti6Al4V tensile specimens

Figure 7 shows the nominal stress-strain curves of the three identical specimens that were obtained after conducting the quasi-static tensile tests. The three curves show good repeatability. From the nominal curves, the $E^*$ was shown to be ~ 118 GPa, yield stress was ~ 944 MPa and $UTS$ was ~ 1058 MPa.

Table 2 shows the true stress and plastic strains according to the specimen2 curve. The Ti64 specimen was ductile, as Fig. 7b shows, because of the obvious necking phenomenon that occurred on the tensile specimen during the tensile test. This conclusion was verified by the fact that the nominal strain of the three specimens was ~ 0.08.

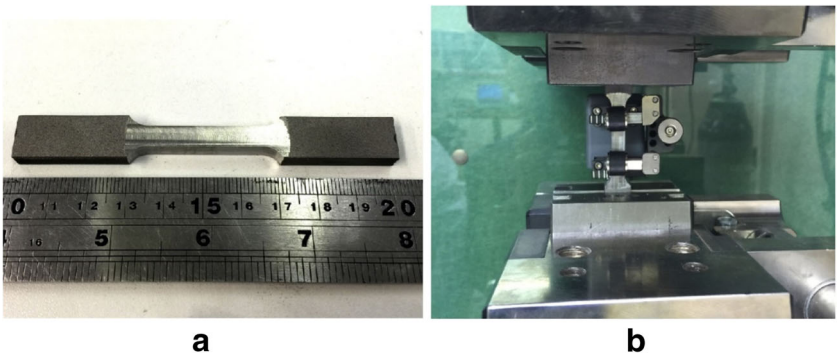


**Fig. 5** **a** SLM-built Ti64 tensile specimen. **b** The quasi-static tensile test

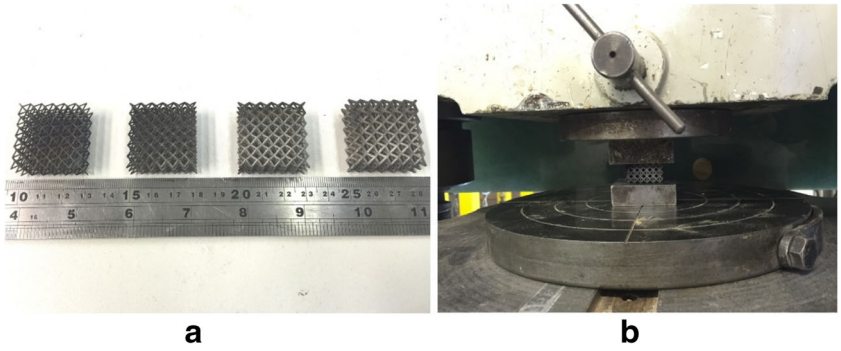


**Fig. 6** **a** SLM-built Ti64 lattice structures. **b** The quasi-static compression test

### 5.2 Stress-strain curves

Figure 8 shows the plotted stress-strain curves of the lattice structures that were obtained from the beam-theory-based Eq. (1) (*Equ*), the proposed quasi-static analysis (*Ana*) and the experimental study (*S1* and *S2*, which represent two identical samples, respectively). For each sub-figure, the number in the title indicates the aspect ratio (AR) of the strut. The elastoplastic properties of these curves were estimated using the following measures. The slope of the linear part of each curve was calculated to be the corresponding equivalent $E^*$. In this study, the *UTS* of each curve that was obtained from quasi-static analysis was prescribed as follows: first, we found the strains corresponded to the *UTS* values of the *S1* and *S2* curves in each sub-figure; second, we found the stress on the *Ana* curve based on the mean value of the above-mentioned two strains.

As Figs. 8 and 9 show, the stress-strain curves for each analytical model began with a steep rise during the elastic stage; in comparison, the curve for each SLM-built lattice structure sample started with a nonlinear curve followed by a steep rise, which resulted from the unstable contact condition during the initial stage of the compression process. The experimental stress-strain curves were sharply reduced after they reached the *UTS* points; no obvious platen phenomenon was observed, which demonstrates that SLM-built Ti64 lattice structures, even when using pre-conducted heat treatment, will show brittleness when they sustain uniaxial compression loads.

The SLM-built Ti64 lattice structures were observed by using an optical microscope, and the actual diameters of the struts of the SLM-built structures are shown in Fig. 10. Table 3 shows the equivalent elastic moduli $E^*$ and *UTS* values of the Ti64 lattice structures that were obtained via the three methods: Eq. (1) (*Equ*), quasi-static analysis (Ana) and experimental tests (S1 and S2). For the BCC-type lattices, when the relative densities increased from 4 to 21%, the $E^*$ values predicted by quasi-static analysis increased from 27 to 1321 MPa, while the *UTS* values predicted increased from 1.7 to 48 MPa. For the fcc-BCC-type lattices, when the relative densities increased from 7 to 33%, the $E^*$ values predicted by quasi-static analysis increased from 316 to 5000 MPa, while the *UTS* values predicted increased from 7.6 to 136 MPa. Hence, we see obvious variations in the mechanical properties of the Ti64 lattice structures as the relative densities vary. In addition, when comparing the $E^*$ and *UTS* values of the BCC-type and fcc-BCC-type lattices with the same strut diameters (or the same aspect ratios), fcc-BCC lattices demonstrated much higher loading capacities, which means that using the superposed-like measure is an effective way to enhance the mechanical properties of Ti64 lattice structures. For example, when the strut diameter ($d$) was 0.54 mm (aspect ratio 8), then the $E^*$ and *UTS* of the BCC lattice predicted by quasi-static analysis were 70 and 4 MPa, while the same values of the fcc-BCC lattice structure were 566 and 14 MPa, respectively.

The diagrams for $E^*$ and *UTS* vs aspect ratio ($l/d$) were then plotted according to the values shown in Table 3, as Fig. 11

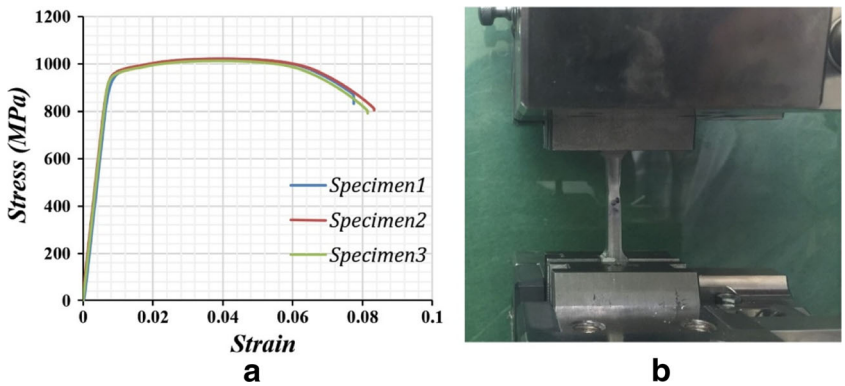


**Fig. 7** **a** Necking phenomenon of a Ti64 tensile specimen. **b** Experimental stress-strain curves of three identical specimens

**Table 2** The true stresses and plastic strains of a Ti64 tensile specimen

| True stress (MPa) | 944 | 973 | 996 | 1015 | 1029 | 1040 | 1047 | 1054 |
|---|---|---|---|---|---|---|---|---|
| True plastic strain | 0 | 0.002 | 0.007 | 0.011 | 0.016 | 0.05 | 0.025 | 0.03 |

shows. The values of the mechanical properties of the structures increased alongside the increase in aspect ratios. The $E^*$ values of both types of structures estimated by quasi-static analysis correlated well with those calculated by the experimental study when the aspect ratio was $l/d \geq 6$ (in the case of slender struts). When $l/d = 4$, this analytical method predicted much larger values compared with those predicted by other analytical measures. The *UTS* values that were predicted by quasi-static analysis agreed well with those predicted by the experimental studies, regardless of whether the struts were slender or thick.

### 5.3 Stress distribution

Figure 12 shows the Von Mises stress distribution of the BCC-type lattice structures when the nominal compressive strains were 0.1, where plastic deformations had occurred in the structures presented in Fig. 8. As Fig. 12 shows, high-stress zones were located in the vicinity of the joints, while low-stress zones were located in the vicinity of the middle of the struts; for example, the stresses near the joints were 1054 MPa, while the stresses near the middle of the struts were only ~ 300 MPa. When the aspect ratios varied from 10 to 4, the high-stress-zone values increased. Another noticeable conclusion that we drew from Fig. 12 is that the deformation of each strut in the lattice structures was homogenous, which demonstrates that the BCC-type structures underwent global deformation rather than local deformation in the strut scale when sustaining compressive loads.

Figure 13 shows the Von Mises stress distributions of the fcc-BCC-type lattice structure; the figure shows that the aspect ratio was 6 when the nominal compressive strains were 0.05, and plastic deformations had occurred in the structures previously shown in Fig. 9. Similarly, to the BCC-type structures, the high-stress and low-stress zones (respectively) were located near the middle of the struts, as Fig. 13a, b shows. The struts in the fcc-BCC unit cells sustained heterogeneous stresses, however. Figure 13c shows a z-plane cut view of Fig. 13b, which shows that nearly all the stresses on the superposed struts (those belong to the superposing FCC unit cell) were ~ 1054 MPa, which indicates that these struts had yielded completely; the other struts belonging to the superposed BCC unit cells presented similar stress distributions as the struts in the BCC lattices shown in Fig. 12 did. Due to the heterogeneity of the strut deformation mentioned above, the fcc-BCC-type lattice structures underwent local deformation within the strut scale.

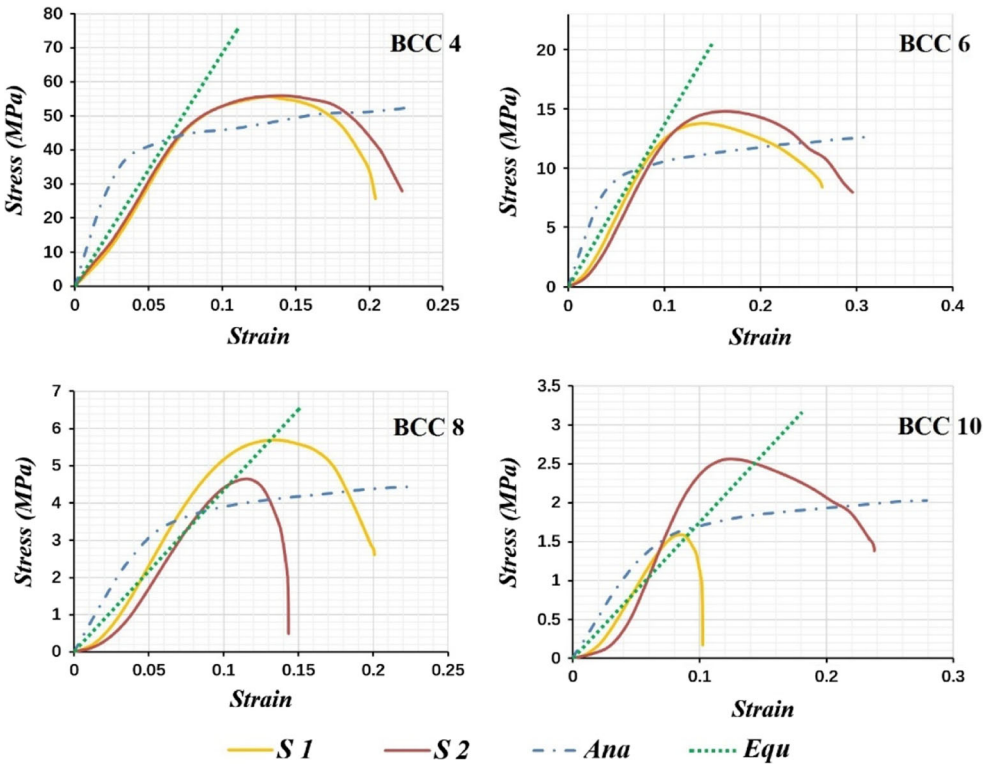


**Fig. 8** Nominal stress-strain curves of BCC lattice structures

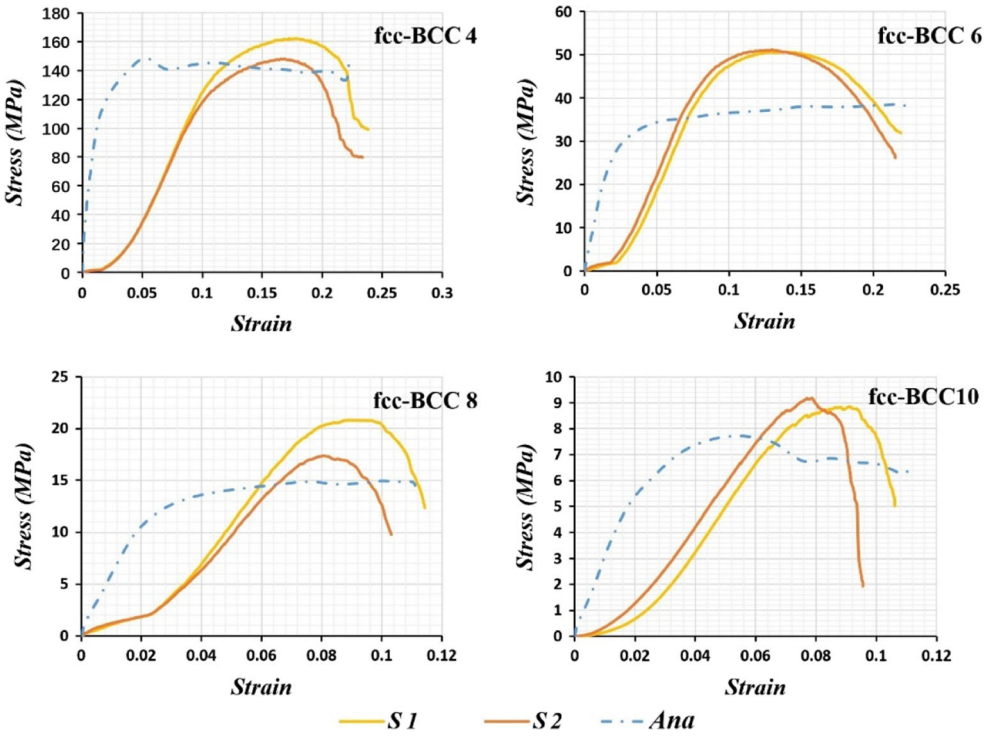


**Fig. 9** Nominal stress-strain curves of fcc-BCC lattice structures

## 6 Discussion

This study has shown that the proposed analytical modelling approach is valid when calculating complex SLM-built Ti64 lattice structures. Although the beam-theory-based theoretical method was able to provide accurate results compared with the testing results, the validity of this method is limited to use with a few structures with simple topologies and straight struts (the BCC type, in this paper). When either (1) the struts in a lattice structure that is consisted of straight struts show different deforming characteristics (as was the case with fcc-BCC in this study), (2) the struts are complicated and curved (e.g. gyroid-type [37]) or (3) unit cells with different topologies exist in a lattice structure (so-called variable-density structures [38]), it becomes quite difficult to calculate the mechanical properties of the lattice structures. The proposed quasi-static analytical method is still practical and accurate, however, and it can theoretically model arbitrary SLM-built structures.

From the results exhibited above, the fcc-BCC type illustrated better lightweight and uniaxial properties than the BCC type. Therefore, this superposing process—by which additional features are superposed to a commonly used unit cell—is a valid and effective method for designing high-performance SLM-built lattice structures with various topologies. The powder-bed nature of the SLM process limits the capability of fabricating the novel structures that are obtained in this process, however. Because, the SLM process requires large enough angles between the surfaces to be melted in the parts and the substrate in the chamber, and the minimum angles will differ according to different metal powders. This superposing process is generally only practical along the

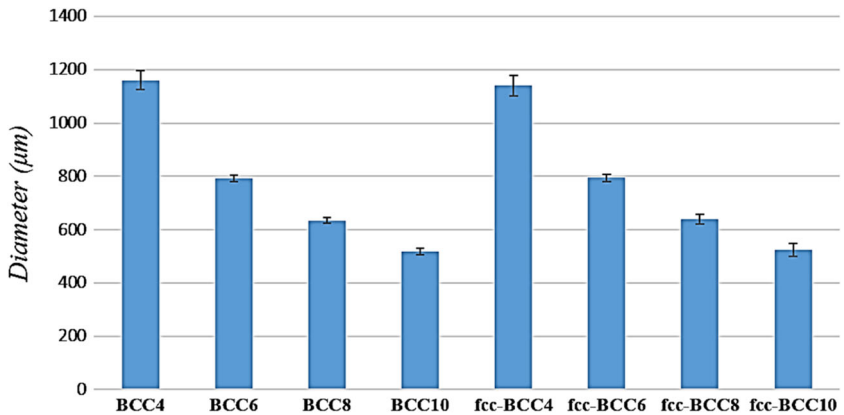


**Fig. 10** Diameters of the struts of the as-produced structures

**Table 3** *E** and *UTS* values of BCC and fcc-BCC Ti64 structures

| Topology | AR | RD (%) | *d* (mm) | | *E** (MPa) | | | | *UTS* (MPa) | | |
|---|---|---|---|---|---|---|---|---|---|---|---|
| | | | CAD | Sample | *Equ* | *Ana* | *S1* | *S2* | *Ana* | *S1* | *S2* |
| BCC | 4 | 21 | 1.08 | 1.16 | 683 | 1321 | 800 | 800 | 48 | 56 | 56 |
| BCC | 6 | 10 | 0.72 | 0.79 | 137 | 220 | 160 | 160 | 12 | 14 | 15 |
| BCC | 8 | 6 | 0.54 | 0.63 | 43 | 70 | 70 | 65 | 4 | 5.7 | 4.6 |
| BCC | 10 | 4 | 0.43 | 0.52 | 18 | 27 | 25 | 50 | 1.7 | 1.6 | 2.55 |
| fcc-BCC | 4 | 33 | 1.08 | 1.14 | – | 5000 | 2800 | 2800 | 136 | 156 | 144 |
| fcc-BCC | 6 | 17 | 0.72 | 0.79 | – | 1400 | 986 | 1000 | 36 | 49 | 50 |
| fcc-BCC | 8 | 10 | 0.54 | 0.64 | – | 566 | 417 | 375 | 14 | 20 | 17 |
| fcc-BCC | 10 | 7 | 0.43 | 0.52 | – | 316 | 260 | 260 | 7.6 | 8.4 | 9 |

uniaxial direction parallel to the build orientation (in this study, for example, the fcc struts were superposed along the y-axis).

Additionally, due to that the strut diameter of the as-produced structures is larger than that of the CAD models, as shown in Fig. 10 and Table 3, the *E** values of the structures should be larger than the analytical results. However, the results show that the proposed quasi-static model predicted higher *E** values of the structures compared with corresponding experimental data, and obvious discrepancies were found when the aspect ratio (AR) is smaller than 6. This contradiction can be attributed to the following reasons. Firstly, the adhered powders increased the diameters of the struts [37], however, due to the properties of lower density; these loose powders did not improve the stiffness of the structures. Moreover, the adhered powder increased the roughness of the as-produced struts, which easily causes the stress concentration and decrease the stiffness of the structures as a consequence. Secondly, when the diameters of the struts are larger (AR ≤ 6), the deformation of the struts are governed by complicated loading conditions including bending, shearing, compressing and stretching. Compared with the case when AR is larger (≥ 8), in which struts can be deemed slender beams and only bending deformation occurred in the structure, complex deformation occurred in the structures with AR ≤ 6 may cause easily complicated stress concentration

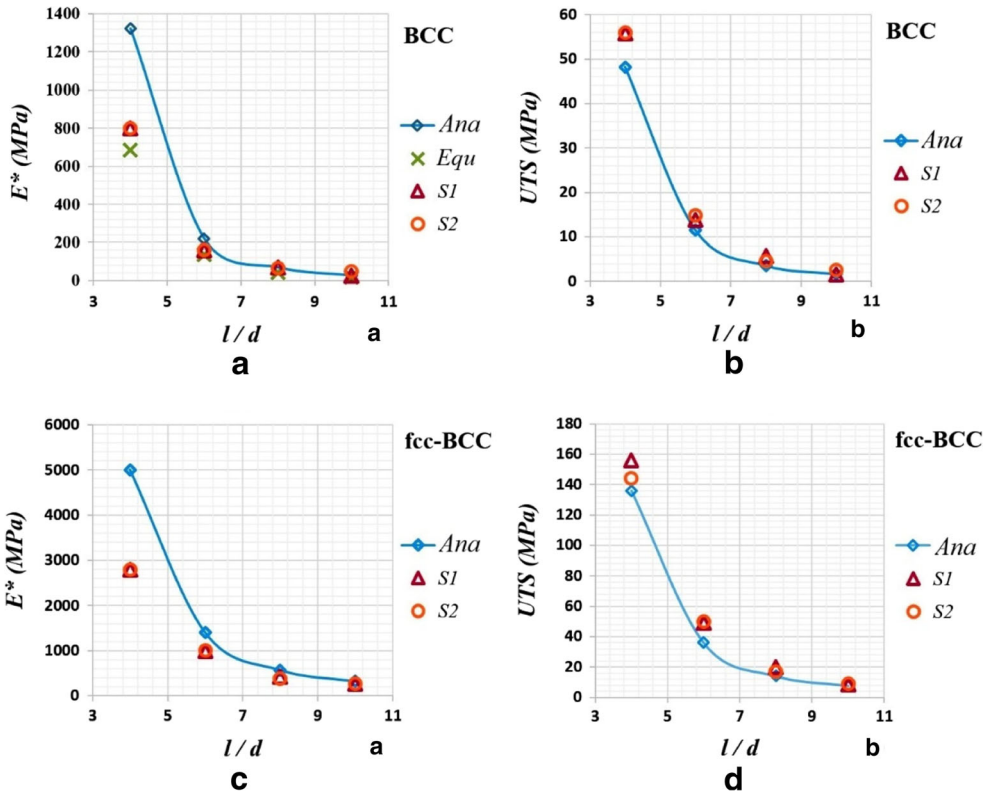


**Fig. 11** *E** and *UTS* vs aspect ratio (*l*/*d*) of the BCC-type and fcc-BCC-type SLM-built Ti64 lattice structures

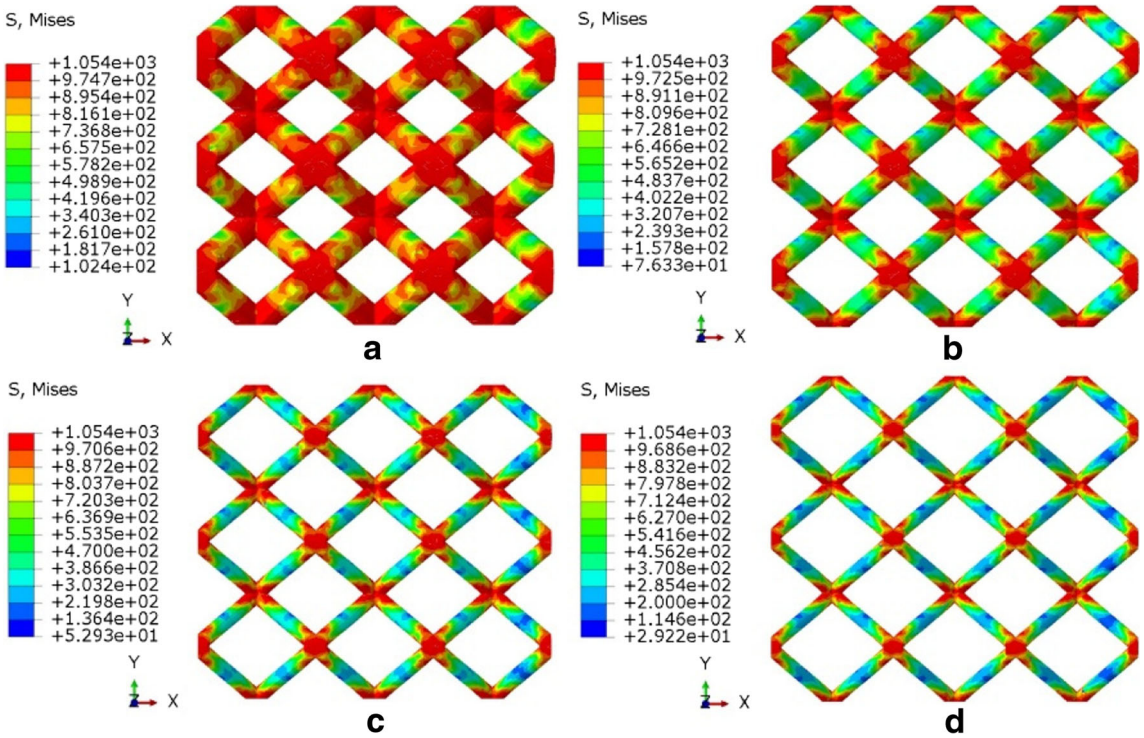


**Fig. 12** Von Mises stress distribution of BCC lattice structures (nominal strain = 0.1). **a** BCC 4. **b** BCC 6. **c** BCC 8. **d** BCC 10

phenomena, which resulted in larger discrepancy between results obtained from the quasi-static analysis and the experimental study.

One of the main challenges of future studies is to improve the process's accuracy by premediating the SLM process's effects on sizes and to decrease the computation time of the quasi-static analysis in order to adapt parts with large scales of unit cells. Another challenge that thus far has puzzled researchers and has impeded wider application of SLM-made metallic lattice structures is that although SLM-built lattice structures are generally simple and symmetric, an effective solution has yet to be proposed for selecting the most suitable structural type to be used in actual applications. In other words, we need to establish a comprehensive method in order to find the optimal lattice structure by considering the structure's mechanical properties, computation and bulk-material costs and the adaptability of the shape of the designed part.

## 7 Concluding remarks

The design of hollow-like Ti64 parts in-filled with lattice structures is an effective solution to decrease the high fabrication costs associated with the current SLM process. In order to estimate the mechanical properties of SLM-built Ti64 lattice structures, this study has first proposed an analytical modelling approach conducting quasi-static analysis on two types of Ti64 lattice structures. It then conducted quasi-static tensile and compression tests in order to calculate essential bulk-material properties and to verify the feasibility of the proposed analytical method. The results are as follows.

1. When the aspect ratios of BCC structures decreased from 10 to 4, the structures' relative densities increased from 4 to 21%. As the results obtained from quasi-static analysis

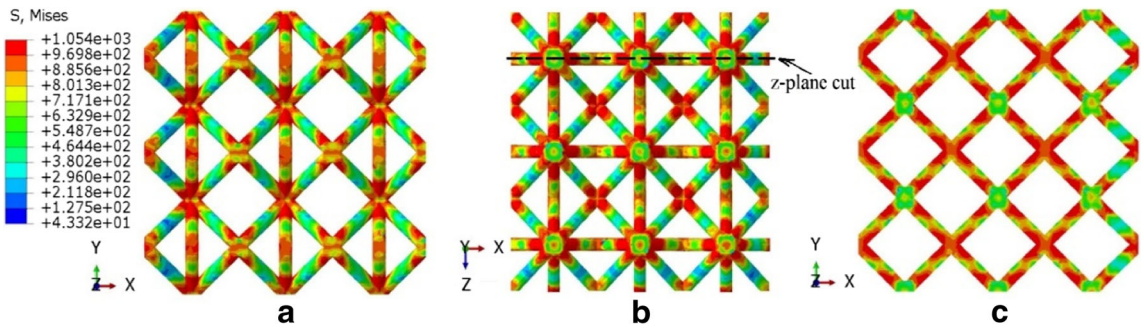


**Fig. 13** Von Mises stress distribution of the fcc-BCC6 structure (nominal strain = 0.05)

showed, the equivalent elastic module ($E^*$) increased from 27 to 1321 MPa, and the ultimate stress (*UTS*) values increased from 1.7 to 48 MPa. These values agreed with the theoretical calculations and the experimental studies when the aspect ratio (*AR*) > 6. In the cases of smaller *AR* values, the *UTS* values were predicted accurately compared with the testing results, while an obvious discrepancy occurred when the *E** values obtained from quasi-static analysis were compared with those of the experimental studies.

2. When the *AR* of fcc-BCC structures decreased from 10 to 4, their relative densities increased from 7 to 33%. The $E^*$ increased from 316 to 5000 MPa, and the *UTS* increased from 7.6 to 136 MPa. The matching quality between the prediction by quasi-static analysis and the testing results was similar to that of the BCC case. The stiffness and strength values of the fcc-BCC structures were three times larger than their counterparts in the BCC structures when their ARs were equal, while their relative densities had increased by less than 80%.
3. The proposed quasi-static analytical modelling approach is valid and effective for use with different kinds of SLM-built Ti64 lattice structures, and, as expected, it can provide guidance when conducting expensive sample tests, thus reducing costs in the designing stage. In addition, when designing SLM-built Ti64 lattice structures, the nature of the powder-bed system should be taken into account before determining the topologies and sizes of the structures. In this way, all the micro-features, such as the struts, can be fabricated successfully (the warping effect is avoided) and accurately (the adhering powders are small enough for the strut sizes).

Although the mechanical properties of a given type of Ti64 lattice structure can be predicted using the proposed analytical method, the design of the hollow-like parts infilled with lattice structures is still difficult to accomplish. Because numerous types of lattice structures have been manufactured due to the manufacturing capacity of the SLM process, designing the best-suited topologies and sizes of the lattice structures in-filled in hollow parts for actual applications is still a time-consuming process that is mainly done by trial and error. This challenge requires a feasible design method that would be suitable for additive manufacturing, which will be examined in follow-up research.

**Acknowledgements** This paper is supported by the Natural Science Foundation of China (Grant No.: 51405046), the Program of International S&T Cooperation (Project No.: 2014DFA73030), and the China Scholarship Council (CSC). The authors would like to thank Ms. Yanlin Wu and Mr. Yipei Liu for their assistance in the development of the analytical method and the experimental study. Sincere thanks are expressed to Chongqing Key Laboratory of Metal Additive Manufacturing (3D Printing) for fabricating the Ti64 samples and also expressed to Cardiff University for the tensile and compression tests shown in this paper.

## References

1. Krishnan M, Atzeni E, Canali R, Calignano F, Manfredi D, Ambrosio EP (2014) Fabrication of three–dimensional honeycomb structure for aeronautical applications using selective laser melting: a preliminary investigation. Rapid Prototyp J 20(6):551–558
2. Mullen L, Stamp RC, Brooks WK, Jones E, Sutcliffe CJ (2009) Selective laser melting: a unit cell approach for the manufacture of porous, titanium, bone in–growth constructs, suitable for orthopedic applications. J Biomed Mater Res B Appl Biomater 89B:325–334
3. Cheng XY, Li SJ, Murr LE, Zhang ZB, Hao YL, Yang R, Medina F, Wicker RB (2012) Compression deformation behavior of Ti–6Al–4V alloy with cellular structures fabricated by electron beam melting. J Mech Behav Biomed Mater 16:153–162
4. Feng Q, Tang Q, Soe S, Liu Y, Setchi R (2016) An investigation into the quasi–static response of Ti6Al4V lattice structures manufactured using selective laser melting. In: Sustainable design and manufacturing. Springer International Publishing, pp 399–409 https://doi.org/10.1007/978-3-319-32098-4_34
5. Zeng L, Xiang N, Wei B (2014) A comparison of corrosion resistance of cobalt–chromium–molybdenum metal ceramic alloy fabricated with selective laser melting and traditional processing. J Prosthet Dent 112(5):1217–1224
6. Read N, Wang W, Essa K, Attallah MM (2015) Selective laser melting of AlSi10Mg alloy: process optimisation and mechanical properties development. Mater Des 65:417–424
7. Han Q, Setchi R, Evans SL (2016) Characterisation and milling time optimisation of nanocrystalline aluminium powder for selective laser melting. Int J Adv Manuf Technol. https://doi.org/10.1007/s00170–016–8866–z
8. Ma M, Wang Z, Gao M, Zeng X (2015) Layer thickness dependence of performance in high–power selective laser melting of 1Cr18Ni9Ti stainless steel. J Mater Process Technol 215(1):142–150
9. Akita M, Uematsu Y, Kakiuchi T, Nakajima M, Kawaguchi R (2016) Defect–dominated fatigue behavior in type 630 stainless steel fabricated by selective laser melting. Mater Sci Eng A 666:19–26
10. Qiu C, Adkins NJE, Attallah MM (2016) Selective laser melting of Invar 36: microstructure and properties. Acta Mater 103:382–395
11. Khan M, Dickens P (2014) Selective laser melting (SLM) of pure gold for manufacturing dental crowns. Rapid Prototyp J 20(6):471–479
12. Zhang X, Xia Y, Wang J, Yang Z, Tu C, Wang W (2015) Medial axis tree—an internal supporting structure for 3D printing. Comput Aided Geom Des 35–36:149–152
13. Deshpande VS, Fleck NA, Ashby MF (2001) Effective properties of the octet–truss lattice material. J Mech Phys Solids 49:1747–1769
14. Wallach JC, Gibson LJ (2001) Mechanical behavior of a three–dimensional truss material. Int J Solids Struct 38:7181–7196
15. Wang J, Evans AG, Dharmasena K, Wadley HNG (2003) On the performance of truss panels with Kagomé cores. Int J Solids Struct 40(25):6981–6988
16. Smith M, Guan Z, Cantwell WJ (2013) Finite element modelling of the compressive response of lattice structures manufactured using the selective laser melting technique. Int J Mech Sci 67:28–41
17. Ding Y, Kovacevic R (2016) Feasibility study on 3–d printing of metallic structural materials with robotized laser–based metal additive manufacturing. JOM 68(7):1–6

18. Cansizoglu O, Harrysson O, Cormier D, West H, Mahale T (2008) Properties of Ti–6Al–4V non–stochastic lattice structures fabricated via electron beam melting. Mat Sci Eng A 492(1–2):468–474
19. Rafi HK, Karthik NV, Gong H, Starr TL, Stucker BE (2013) Microstructures and mechanical properties of ti6al4v parts fabricated by selective laser melting and electron beam melting. J Mater Eng Perform 22(12):3872–3883
20. Arabnejad S, Johnston RB, Ann J, Singh B, Tanzer M, Pasini D (2016) Acta Biomaterialia high–strength porous biomaterials for bone replacement: a strategy to assess the interplay between cell morphology, mechanical properties, bone ingrowth and manufacturing constraints. Acta Biomater 30:345–356
21. Yavari SA, Ahmadi SM, Stok JVD, Wauthle R, Riemslag AC, Janssen M, Schrooten J, Weinans H, Zadpoor AA (2014) Effects of bio–functionalizing surface treatments on the mechanical behavior of open porous titanium biomaterials. J Mech Behav Biomed Mater 36:109–119
22. Yavari SA, Wauthle R, Stok JVD, Riemslag AC, Janssen M, Mulier M, Kruth JP, Schrooten J, Weinans H, Zadpoor AA (2013) Fatigue behavior of porous biomaterials manufactured using selective laser melting. Mater Sci Eng C 33(8):4849–4858
23. Yavari SA, Ahmadi SM, Wauthle R, Pouran B, Schrooten J, Weinans H, Zadpoor AA (2015) Relationship between unit cell type and porosity and the fatigue behavior of selective laser melted meta–biomaterials. J Mech Behav Biomed Mater 43:91–100
24. Sallica-Leva E, Jardini AL, Fogagnolo JB (2013) Microstructure and mechanical behavior of porous Ti–6Al–4V parts obtained by selective laser melting. J Mech Behav Biomed Mater 26:98–108
25. Sun J, Yang Y, Wang D (2013) Mechanical properties of a Ti6Al4V porous structure produced by selective laser melting. Mater Des 49: 545–552
26. Wauthle R, Vrancken B, Beynaerts B, Jorissen K, Schrooten J, Kruth JP, Humbeeck JV (2015) Effects of build orientation and heat treatment on the microstructure and mechanical properties of selective laser melted Ti6Al4V lattice structures. Addit Manuf 5:77–84
27. Song B, Dong S, Liao H, Coddet C (2012) Process parameter selection for selective laser melting of Ti6Al4V based on temperature distribution simulation and experimental sintering. Int J Adv Manuf Technol 61(9):967–974
28. Santos EC, Osakada K, Shiomi M, Kitamura Y, Abe F (2004) Microstructure and mechanical properties of pure titanium models fabricated by selective laser melting. Proc Inst Mech Eng C J Mech Eng Sci 218:711–719
29. Hasan R, Mines R, Fox P (2011) Characterization of selectively laser melted Ti–6Al–4V micro–lattice struts. Procedia Eng 10: 536–541
30. Qiu C, Yue S, Adkins NJE, Ward M, Hassanin H, Lee PD, Withers PJ, Attallah MM (2015) Influence of processing conditions on strut structure and compressive properties of cellular lattice structures fabricated by selective laser melting. Mat Sci Eng A 638(18): 228–231
31. Sing SL, Yeong WY, Wiria FE, Tay BY (2016) Characterization of titanium lattice structures fabricated by selective laser melting using an adapted compressive test method. Exp Mech 56(5):735–748
32. Bael SV, Kerckhofs G, Moesen M, Pyka G, Schrooten J, Kruth JP (2011) Micro–CT–based improvement of geometrical and mechanical controllability of selective laser melted Ti6Al4V porous structures. Mater Sci Eng A 528(24):7423–7431
33. Mazur M, Leary M, Sun S, Vcelka M, Shidid D, Brandt M (2015) Deformation and failure behaviour of Ti–6Al–4V lattice structures manufactured by selective laser melting (SLM). Int J Adv Manuf Technol 84:1391–1411
34. Ushijima K, Cantwell W, Mines R, Tsopanos S, Smith M (2011) An investigation into the compressive properties of stainless steel micro–lattice structures. J Sandw Struct Mater 13(3):303–329
35. Ushijima K, Cantwell WJ, Chen DH (2013) Prediction of the mechanical properties of micro–lattice structures subjected to multi–axial loading. Int J Mech Sci 68:47–55
36. Gümrük R, Mines RAW (2013) Compressive behaviour of stainless steel micro–lattice structures. Int J Mech Sci 68:125–139
37. Yan C, Hao L, Hussein A, Raymont D (2012) Evaluations of cellular lattice structures manufactured using selective laser melting. Int J Mach Tools Manuf 62:32–38
38. Zhang P, Toman J, Yu Y, Biyikli E, Kirca M, Chmielus M, To AC (2014) Efficient design–optimization of variable–density hexagonal cellular structure by additive manufacturing: theory and validation. J Manuf Sci Eng 137:021004
39. Aremu AO, Maskery C, Tuck C, Ashcroft IA, Wildman RD, Hague RIM (2014) A comparative finite element study of cubic unit cells for selective laser melting. In SFF: 1238-1249. http://sffsymposium.engr.utexas.edu/sites/default/files/2014-097-Aremu.pdf